TagSense: Robust Wheat Moisture and Temperature Sensing Using RFID

Erbo Shen, Weidong Yang, *Member, IEEE*, Xuyu Wang, *Member, IEEE*, Bo Kang, and Shiwen Mao, *Fellow, IEEE*

***Abstract*—Grain is a major source of food, while grain security has been considered as a strategic issue in many countries. Temperature and moisture as the two key properties affect the quality of stored grain. Most existing approaches for sensing these properties are expensive, time-consuming, and are difficult to deploy. In this paper, we design a TagSense system to sense the temperature and moisture level of stored wheat using commodity RFID devices, where tag's impedance is exploited as a feature for target sensing at a low cost. Since impedance is sensitive to the signal propagation distance and incidence angle, we propose a distance-independent algorithm and an angle-agnostic approach to mitigate the impact of distance and angles on the sensing performance. Our extensive experiment results demonstrate that TagSense can achieve a satisfactory sensing performance at any distance and any angle within the sensing range.**

***Index Terms*—Radio frequency identification (RFID), radio frequency (RF) sensing, target properties sensing, multi-class support vector machine (SVM).**

I. Introduction

With the rapid growth of the global population and the improvement of consumption level, the demand for grain will be doubled by the year of 2050 [1]. There is a compelling need for an effective method to preserve surplus food to meet the increasing future demand and to prepare for unexpected events such as war, natural disaster, pandemic, or drought. Thus, grain storage becomes highly important for national security. Temperature and moisture as the two key properties of stored grain that largely determine the safety of grain. Therefore, how to monitor these two factors accurately and effectively is of great importance.

The existing grain moisture detection methods belong to the drying method [2], the capacitance method [3], the electromagnetic microwave method [4], the resistance method [5], and the neutron gauge method [6]. Most methods are contactful, which is usually time-consuming, inefficient, and costly. For temperature measurement, various wired sensors are inserted into the wheat pile to measure the physical characteristics. However, once deployed, these devices are hard to replace if one node fails to work. It is also inconvenient to update and upgrade these sensors. The traditional measurement methods also do not meet the requirement of high accuracy for both temperature and moisture sensing. An effective solution of low power consumption, low cost, easy deployment, and high accuracy would be highly appealing.

Our early works have used WiFi-CSI signals for contactless target sensing [7], [8], [9]. However, WiFi-CSI signals are easily influenced by environmental dynamics (e.g., movements of the other objects in the surroundings), which could weaken the robustness of the RF sensing system. Compared with WiFi CSI based systems, RFID based sensing technologies have the unique advantages of small form factor and low cost. RFID is also more resilient to environmental interference [10]. Therefore, it has been used in many IoT applications, such as healthcare [11], material identification [12], vibration sensing and identification [13], intelligent identification [14], localization [15], [16], and human movement detection [17], touch gesture and motion tracking [18], material recognition [19], [20], moisture measurement [21], [22], [23], [24], material temperature sensing [20], [25], [26], [27], [28], [29] and smart architecture [30]. Most of the applications leverage phase, phase difference, or signal strength to sense the target's properties, and have achieved a promising performance. However, RFID phase and phase difference are sensitive to the environment dynamics such that it is hard to ensure a stable sensing performance. To this end, this paper proposes to use *RFID tag impedance* to sense the target properties. We show that the variation in RFID tag impedance is a major factor that causes phase changes. Therefore, we find that the impedance can better capture the physical mechanisms behind sensing. More important, the tag impedance is easier to obtain and is more stable than phase or phase difference. Therefore, we propose to leverage the tag impedance for sensing the temperature and moisture level of stored wheat.

Manuscript received 5 January 2024; revised 13 March 2024; accepted 12 April 2024. Date of publication 16 April 2024; date of current version 3 May 2024. This work was supported in part by the National Science Foundation of Henan under Grant 222300420004, and in part by the Major Public Welfare Special Projects of Henan Province under Grant 201300210100. A preliminary version of this work was presented in part at IEEE ICC 2022, Seoul, South Korea, May 2022 [DOI: 10.1109/ICC45855.2022.9838925]. *(Corresponding author: Weidong Yang.)*

Erbo Shen is with the Henan Key Laboratory of Grain Photoelectric Detection and Control, Henan University of Technology, Zhengzhou 450001, China, and also with the College of International Education, Kaifeng University, Kaifeng 475001, China (e-mail: shenbo412@163.com).

Weidong Yang and Bo Kang are with the Henan Key Laboratory of Grain Photoelectric Detection and Control, Henan University of Technology, Zhengzhou 450001, China (e-mail: yangweidong@haut.edu.cn; 504104474@qq.com).

Xuyu Wang is with the Department of Computer Science, Florida International University, Miami, FL 33199 USA (e-mail: xuywang@fiu.edu).

Shiwen Mao is with the Department of Electrical and Computer Engineering, Auburn University, Auburn, AL 36849 USA (e-mail: smao@ieee.org).

Digital Object Identifier 10.1109/JRFID.2024.3389868

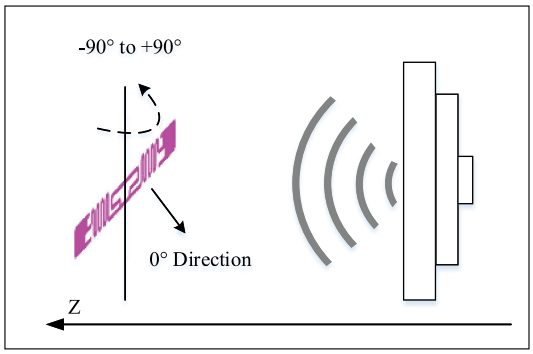

Fig. 1. The tag faces the Z-axis (the incident direction of the EW) and rotates 180° from −90° to +90°.

However, there remain many challenges for RFID-based wheat moisture and temperature sensing. *The first challenge* is the multipath signal propagation. In RFID communication systems, the Electromagnetic Wave (EW) (e.g., RFID signal) from the transmitter can propagate to the receiving end through multiple paths, resulting in multipath interference. Effective methods are needed to process the multi-path signals to obtain clean signals. *The second challenge* is that the tag impedance is highly dependent on the sensing range. Thus, we need to eliminate the impact of distance on the measured impedance. *The third challenge* is the interference of penetrating signal. Generally, wireless EW has a strong penetration ability. It leads to an additional interference signal in the measured impedance, which increases the complexity of the system. *The fourth challenge* is from the random sensing angles. In practical applications, the target may be placed randomly in the sensing area, while various sensing angles affect the measured impedance.

To address the first two challenges, we choose the relatively 'cleaner' channels in resonance frequencies within 860 MHz to 960 MHz to collect RF data. Then, a distance-independent algorithm is developed to reduce the impact of multi-path interference and distance dependence. To address the third challenge, consider the setup shown in Fig. 1, where the z-axis represents the direction of the EW.The RFID tag is put in front of the reader antenna at line-of-sight (LOS) with the angle ranging from −90° to +90°. This way, the interference of penetrating signals can be mitigated. In addition, we place a microwave absorbing sponge behind the wheat sample to further reduce the interference of the penetrating signal. To address the fourth challenge, we utilize a circularly polarized antenna with a beamwidth 65°, which helps to greatly reduce the sensitivity to direction. Also, the tag's impedance periodically changes as it rotates like a cosine function. We use a multi-class support vector machine (SVM) to identify rotation angles to reduce the impact of sensing angle.

In this paper, we propose the TagSense system, which is a novel target sensing system designed for monitoring the temperature and moisture level of stored wheat [31]. The unique advantage of TagSense is that we do not need to attach the tag to the target tightly, but just put the tag on a bag, a box, or other containers. TagSense can sense the material properties within the container, including moisture level and temperature. Within the maximum sensing range, TagSense can work well at any specific sensing distance or angle. Unlike existing systems [32] that use customized hardware or specially designed high-frequency signals to sense material, TagSense uses tag's impedance and resonance frequency that is easy to measure at a low cost. The deployment of TagSense is easy with COTS RFID tag, in which the S-parameter and frequency are displayed on a computer from a Vector Network Analyzer (VNA) device.

To make TagSense robust, we design a distance-independent algorithm and an angle-agnostic approach to allow effective sensing of wheat samples at any distances and any angles within the range. This study provides a novel method to achieve robust sensing of target's properties with cheap COTS devices. The three contributions of this work are summarized as follows.

- We take stored wheat as the sensing target, and achieve robust sensing of temperature and moisture level using tag's impedance with a single passive RFID tag. This is a novel approach that leverages tag impedance for simultaneously determining the target's temperature and moisture.
- In order to obtain robust impedance measurements at any distance and any angle, we present a distance-independent algorithm based on EW reflection theory and an angle-agnostic method utilizing a multi-class support vector machine (SVM).
- We conduct extensive experiments with real stored wheat in various scenarios. The efficacy, accuracy, and robustness of TagSense are verified.

The remainder of this paper is structured as follows. In Section II, we introduce a study of RFID tag modeling and discuss the challenges on system design. We present the framework of TagSense in Section III and evaluate its performance in Section IV. Section V concludes this paper.

II. Preliminary Study and Design Challenges

In this section, we present our preliminary study of RFID sensing and the feasibility of the TagSense system. We also examine how the surroundings impact the system performance. Finally, we describe two challenges that need to be addressed in the TagSense system design.

A. Preliminary Study

An RFID Tag consists of two parts, i.e., the chip and the tag antenna connected to the chip. Its impedance can be represented by an equivalent impedance, which is the ratio of the complex voltage to complex current at a certain point on the transmission line. Tag's impedance is related to the incident and reflected wave, and can be expressed using the S-parameter, which, however, is difficult to be determined with the S-parameter directly. To assess the tag's sensitivity to the surroundings, we introduce a measurement method of tag antenna impedance based on the S-parameter. This will indirectly reveal the mechanism by which the tag senses the target. We will approximate the tag's impedance by introducing the concept of equivalent load impedance and

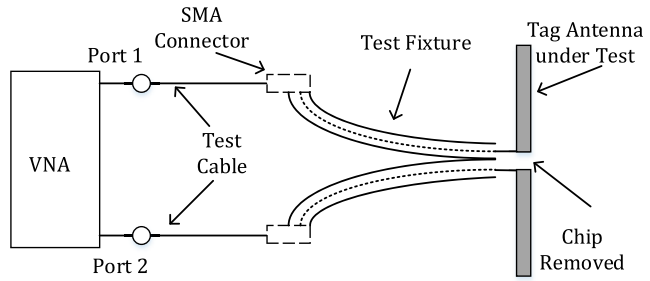

(a) Connection between the tag antenna and the VNA device.

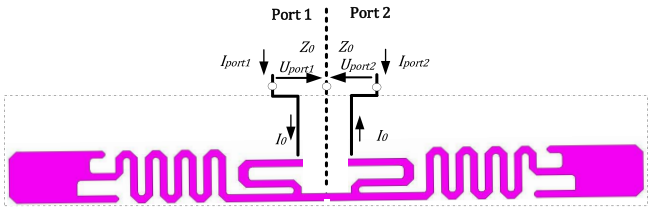

(b) Measuring the tag antenna impedance.

Fig. 2. Illustration of how to measure the tag antenna impedance based on the S-parameter. The chip is removed from the tag.

present the relationship between the tag antenna impedance and the tag's impedance, which will be discussed in detail in the following.

1) Tag Antenna Impedance: We present a measurement method of tag antenna impedance based on the measured S-parameter using a VNA device. The goal is to test the sensitivity of the tag when it is used to sense the environment, which will validate the feasibility for using RFID tags to sense targets at different temperatures and moisture levels.

First, the chip is removed from RFID tag, while the two ports of the antenna are each connected to one of the two ports of the VNA. The VNA will then measure the S-parameter of the tag antenna, which will be used to obtain the tag antenna impedance, as shown in Fig. 2(a). More details can be found in [33]. In the figure, SMA represnts Sub-Miniature-Version-A, which is used for the connection between the test fixture and the test cable to the VNA device. Fig. 2(b) illustrates the measurement method, where I_{port1} and I_{port2} respectively denote the current received from the two ports of the VNA, U_{port1} and U_{port2} denote the voltages of the two ports, respectively, and Z_0 is the characteristic impedance of the ports (i.e., 50Ω).

We define the tag antenna impedance as the equivalent impedance at the input port. If current is denoted by I_0 and voltage by U, the impedance Z_d is dependent on the S-parameter [33]. Tag antenna impedance is given by $Z_d = (U_{port1} - U_{port2})/I_0$. Based the Z-parameters [34], we have

$$\begin{cases} U_{port1} = Z_{11} I_{port1} + Z_{12} I_{port2} \\ U_{port2} = Z_{21} I_{port1} + Z_{22} I_{port2}, \end{cases} \tag{1}$$

where matrix $\{Z_{ij}\}$ consists of impedance coefficients: Z_{11} is the forward transfer impedance of Port 1 when Port 2 is open, Z_{12} is the reverse transfer impedance when Port 1 is open, Z_{21} is the forward transfer impedance when Port 2 is open, and Z_{22} is the impedance of Port 2 when Port 1 is open. Considering $I_{port1} = I_0$ and $I_{port2} = -I_0$, we have $U_d = U_{port1} - U_{port2} = (Z_{11} - Z_{21} - Z_{12} + Z_{22})I_0$, and the impedance of the tag antenna is given by

$$Z_d = \frac{U_d}{I_0} = (Z_{11} - Z_{21} - Z_{12} + Z_{22}). \tag{2}$$

The Z-parameters are related to S-parameters as [35]

$$Z_d = \frac{2Z_0(1 - S_{11}S_{22} + S_{12}S_{21} - S_{12} - S_{21})}{(1 - S_{11})(1 - S_{22}) - S_{21}S_{12}}, \tag{3}$$

where $Z_0 = 50\ \Omega$ is the characteristic impedance related to the cables used for measurement. For a symmetric, balanced tag antenna, i.e., $S_{11} = S_{22}$ and $S_{12} = S_{21}$, we have

$$Z_d = \frac{2Z_0\left(1 - S_{11}^2 + S_{21}^2 - 2S_{21}\right)}{(1 - S_{11})^2 - S_{21}^2}, \tag{4}$$

where S_{11} and S_{21} denote the reflection corresponding to Port 1 and Port 2, respectively, which can be obtained from the VNA. Since the tag antenna is connected to the two VNA ports, the distance from tag to transmitting antenna (i.e., the RFID reader antenna) is not considered here. Thus, the tag antenna impedance can be obtained by (4).

2) Impedance Variations Caused by Surroundings: We next show how the surroundings affect tag antenna impedance. Specifically, we consider temperature and the distance from tag to reader antenna as two major factors that affect the tag antenna impedance.

To study how temperature affects tag antenna impedance, we attach an RFID tag to the container that holds the wheat samples, and put the wheat sample in a refrigerator to freeze it to −10°C. We observe and record the S-parameter when temperature gradually rises from −10°C to 20°C, and calculate the tag antenna's impedance using (4). From Fig. 3(a), we find that the impedance clearly changes with temperature following a strong linear relationship [28].

Next, we put the tag antenna at, and then far away from the wheat sample, to observe the impact of distance on tag antenna impedance. Fig. 3(b) and Fig. 3(c) show the changes in the real and imaginary parts of the measured tag antenna impedance over different frequencies, respectively, when the tag antenna is placed at and away from the wheat. We find that both real parts (near and far) decrease with the increase of frequency, and both imaginary parts exhibit an increasing trend with the increase of frequency. Through the above experiments, we conclude that tag antenna impedance is sensitive to both temperature and distance.

B. System Design Challenges

In the previous study, the tag antenna impedance is measured by directly attaching an SMA to the tag antenna. In practice, (i) the distance between the tag antenna and the SMA, and (ii) the angle of the tag with respect to the reader antenna, pose two challenges for designing a robust system.

The purpose for testing the impedance of chip-less tags is to verify their sensitivity to environmental factors, such as temperature and moisture. However, in practical applications, there are distances between tag (with chip) and RFID reader that is different from the scenario in Section II-A. Therefore,

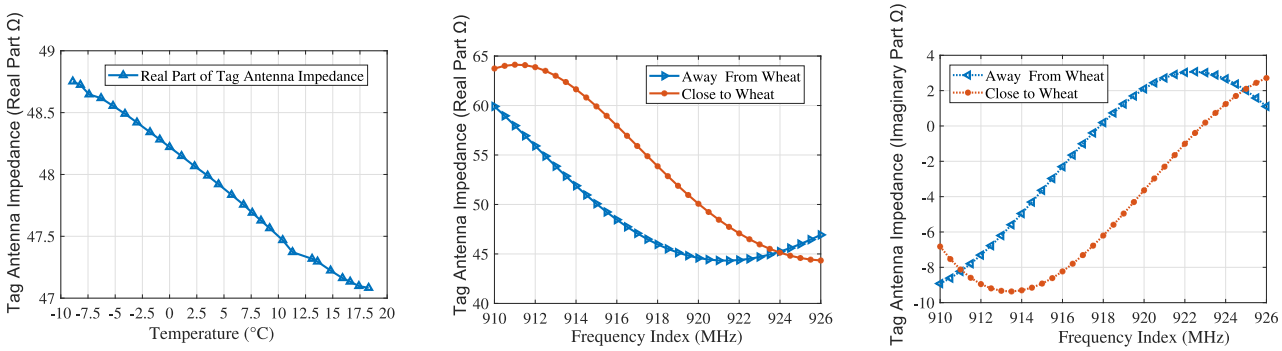

(a) Real part of tag antenna impedance versus temperature.

(b) Real part when the tag antenna is close to or far away from the tag.

(c) Imaginary part when the tag antenna is close to or far away from the tag.

Fig. 3. How the tag antenna impedance is affected by the surrounding temperature and tag-antenna distance.

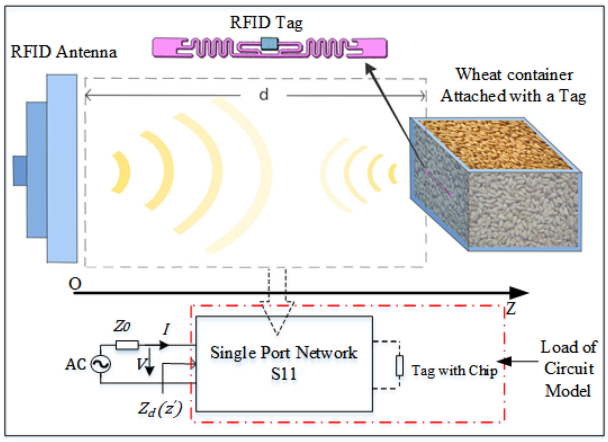

Fig. 4. Illustration of a typical TagSense deployment scenario and the equivalent circuit model. Load impedance measurement is based on the reflection coefficient. For a single port network, the impedance $Z_d(z')$ is a function of the tag position z'.

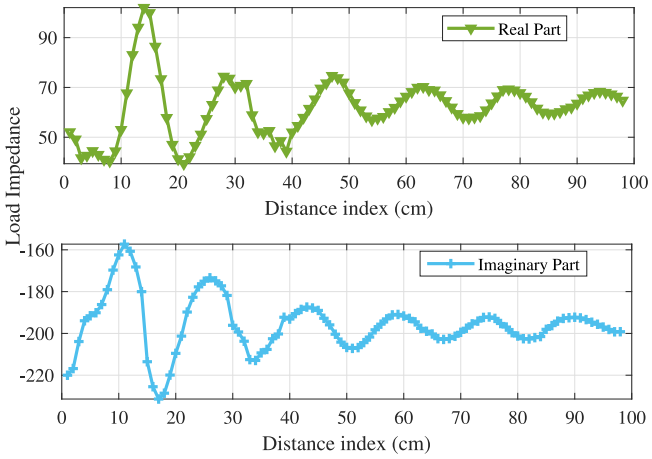

Fig. 5. The tag impedance changes periodically at a period of $\lambda/2$.

in the following, we will first propose an equivalent circuit model for tag (with chip) based sensing system to illustrate the parallel impedance between tag antenna and chip, and then examine these two challenges in detail. Note that tag refer to tag with chip in the subsequent sections.

1) The Equivalent Circuit Model of TagSense : Fig. 4 illustrates a practical scenario where TagSense is deployed, along with the equivalent circuit model. The tag attached to the wheat box communicates with the reader antenna over a distance. The channel between the tag and reader antenna can be equivalent to a transmission line (i.e., a lossy medium), and the tag, along with its surroundings (wheat moisture and temperature), can be considered as an RF terminal. The transmission line and RF terminal function as the load of the circuit model, marked by the red dashed box in the figure. Fig. 4 also illustrates the model of EW propagation with the equivalent circuit model, where parameter O represents the input and output ports of the load, d is the distance from tag to reader antenna (i.e., the transmitting antenna), AC denotes the source of wireless signal, I is the current measured by the Single Port Network, V denotes the voltage, and z' is the position of the tag (wheat sample) along the Z-axis.

2) Distance Dependence: With the transmission line model, we can capture the relationship of load impedance and distance d as follows.

$$S_{11}(z') = \frac{Z_d(z') - Z_0}{Z_d(z') + Z_0}, \tag{5}$$

where S_{11} denotes the reflection coefficient at O, which can be read from the analog VNA/reader device as a complex number, $Z_d(z')$ denotes the load impedance at position z', and Z_0 denotes the tag chip's impedance, which is $(28.3 - j204.2)\Omega$. When S_{11} is a constant, the load impedance $Z_d(z')$ is directly related to position z'. By introducing the equivalent circuit model, the load's impedance can be directly obtained from (5).

Fig. 5 shows the circuit's load impedance obtained at a frequency of 960 MHz. The impedance periodically changes with distance d, at a period of half of the wavelength (i.e., $\lambda/2$). The impedance amplitude decreases with increased distance d, and the signal attenuation increases rapidly after the first wavelength. It can also be seen in Fig. 5 that the real and imaginary curves exhibit similar trends, except that the real part lags $\pi/4$ behind the imaginary part.

To make TagSense more robust, the impact of distance d should be effectively mitigated. We will present

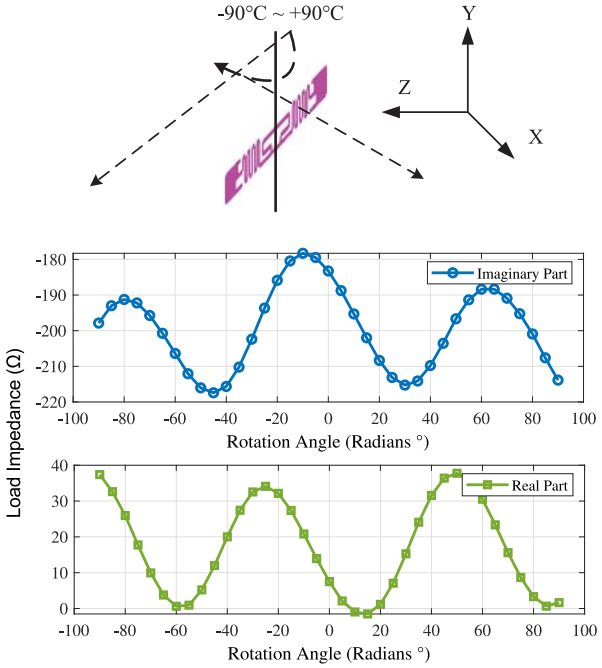

Fig. 6. When the tag rotates from $-\pi/2$ to $+\pi/2$, the load impedance (both real part and imaginary part) changes periodically.

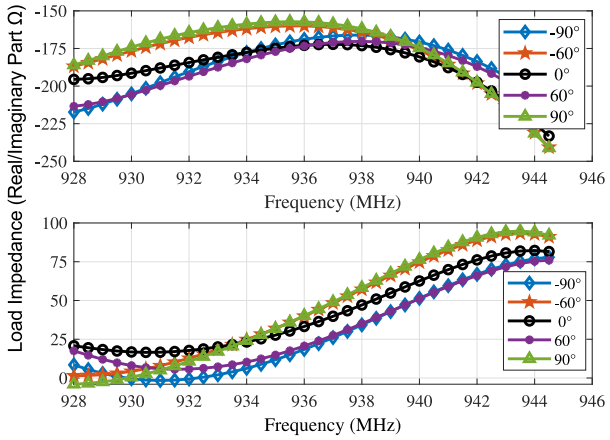

Fig. 7. Effect of the tag rotation angle on tag impedance at different frequencies.

a distance-independent algorithm based on the Fresnel-reflection-coefficient in Section III-D to address this issue.

3) Angle Interference: Next we examine how the angle of the tag (with respect to the reader antenna) affects the impedance measurement. We place the wheat container (made of organic glass) at random angles, and observe the change in load impedance. Fig. 6 shows that the load impedance (both the Real Part and Imaginary Part) changes periodically with the angle at a period of $4\pi/5$.

We also examine the effect of frequency on load impedance. Fig. 7 shows how the impedance changes when frequency is increased from 928 MHz to 945 MHz and the tag angle is at $\{-\pi/2, -\pi/3, 0, +\pi/3, +\pi/2\}$. It is noticed that the curves at certain angles are very close (e.g., $-\pi/3$ and $+\pi/2$, and $+\pi/3$ and $-\pi/2$). Through the above observations, it can be concluded that the tag angle affects the robustness of

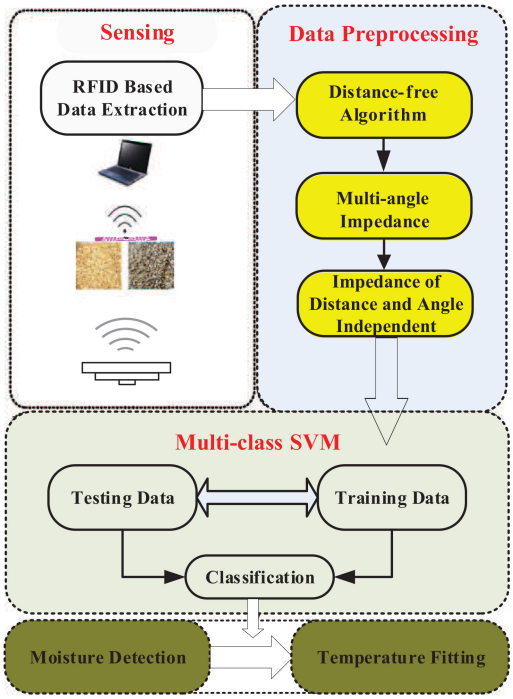

Fig. 8. System architecture of TagSense.

TagSense. We will propose an angle-agnostic method based on a multi-class SVM to address the angle dependence problem in Section III-E.

III. The TagSense System Design

We present the design of TagSense in this section, which is a radio frequency (RF)-based wheat moisture and temperature sensing method using COTS RFID. We shall propose a three-layer model for the RFID transmission process, followed by the distance-independent algorithm and the angle-agnostic method. Finally, we present the temperature and moisture sensing methods.

A. TagSense Architecture

The TagSense system consists of a VNA/reader device connected to a reader antenna through a cable, and a passive tag attached to the container of wheat. A copper plate is attached to the back side of the container. The VNA/reader device queries the tag, and receives the tag response from the antenna to extract useful information. A desktop computer is connected to the VNA/reader to analyze and visualize the sensory data. Fig. 8 illustrates the architecture of TagSense, which includes four parts: (i) RF data acquisition, (ii) data pre-processing, (iii) multi-class SVM based classification, and (iv) moisture level and temperature sensing.

Specifically, when the tag is activated by the EW from the reader antenna, it generates a response signal, which is received by the reader antenna and sent to the VNA/reader device. Then the VNA/reader device obtains the S-parameters and resonance frequency, which are sent to the computer for preprocessing. The data preprocessing module calculates the load of circuit model to obtain a stable impedance

measurement using the proposed angle-agnostic and distance-independent algorithms. Finally, the moisture level and temperature of the wheat sample are derived from the measured impedance data.

B. RF Data Collection

1) Sensing Distance: For data acquisition, the reader antenna transmits EW to the sensing space. The Tag is activated after receiving the EW, and then returns a response signal back to the VNA/reader. The S-parameter and frequency of the response are then measured by the VNA/reader device, and sent to desktop for pre-processing.

In this module, the maximum sensing distance R is a key factor, which can be obtained by

$$R = \frac{\lambda}{4\pi}\sqrt{\frac{P_{Re}G_{Tr}G_{Re}\tau}{P_{Th}}}, \tag{6}$$

where G_{Tr} and G_{Re} denote the gain of the transmitting and receiving antennas, respectively, P_{Re} denotes the energy of the tag reflected signal, τ denotes the transmission coefficient, and P_{Th} denotes the threshold power of the micro chip. According to the hardware configuration of the system, the theoretical sensing distance is about 10 m.

2) Dataset Collection: We first record the impedance when the rotation angle is set to 0°, which is used as the target of training. Second, we rotate the wheat container along with the attached tag from $-\pi/2$ to $\pi/2$, as shown in Fig. 1, and record the impedance for every 5°. A total of 37 impedance values are recorded. Between the frequency of 860 MHz and 960 MHz, impedance samples are recorded every 0.5 MHz. Thus we obtain a total of 201 samples. Then, we record impedance per 1 cm when the distance d is increased from 3 cm to 100 cm, and a total of 98 samples are recorded. In the same way, we record six groups of wheat samples at different moisture levels, and repeat the above steps for 20 times for each group to obtain more training samples. Last, a total of 87,459,120 data samples are obtained (10 (moisture levels) $\times$37 (rotation angels) $\times$201 (frequencies) $\times$98 (distances) $\times$20 (repeated times)).

Furthermore, we choose one or two "clean" channels out of the 201 frequencies. We randomly divide the chosen dataset into three parts, where 60% of samples are for training, 20% are trained after adding noise to enhance the robustness, and 20% are used for testing.

C. Three-Layer Model

We propose a three-layer model to better describe the EM transmission and scattering process in different mediums. Consider the air, tag and wheat, and the copper plate as three different layers of media, in which the EW propagates, scatters, and reflects at the boundary of different layers with different dielectrics, as shown in Fig. 9. We assume the Fresnel reflection coefficient and transmission coefficient of the copper plate as -1 and 0, respectively, which means that the signal will be completely reflected on the surface and nothing will go through the copper plate. Let Ef_{1i}, H_{1i}, and K_{1i} denote the incident electric field, incident magnetic field, and direction of wave propagation in layer 1, respectively; Ef_{1r}, H_{1r}, and

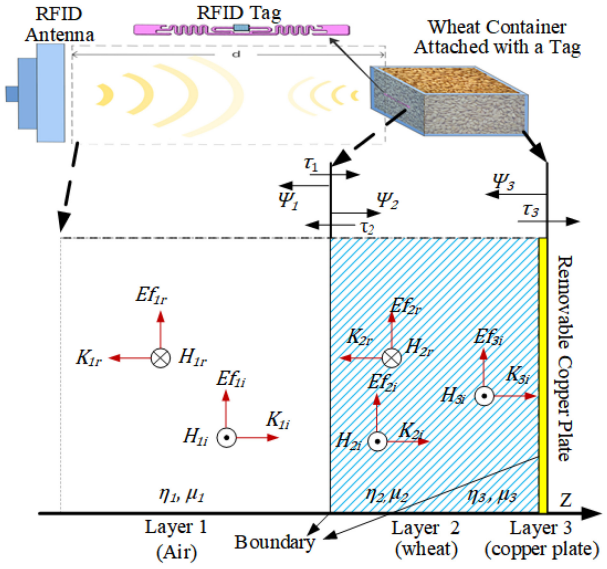

Fig. 9. The three-layer model consisting of the open space between the reader antenna and tag, the wheat with a tag, and the copper plate placed at the back side of the container. The tag's impedance is obtained by the Fresnel reflection coefficient.

K_{1r} denote the reflected counterparts in layer 1, respectively. The electromagnetic waves in layer 2 and layer 3 are defined similarly. The copper plate placed behind the container can be removed according to the experimental requirements.

Let μ_i denote the permeability of layer i with dielectric constant η_i, $i = 1, 2, 3$. In Fig. 9, Ψ_1 denotes the Fresnel reflection coefficient of the boundary from layer 1 to layer 2, which is also the tag's reflection coefficient. The tag's transmission coefficient is τ_1. Moreover, the corresponding parameters for the interface from layer 2 to layer 1 are Ψ_2 and τ_2, respectively; and for the interface from layer 2 to layer 3, the corresponding parameters are Ψ_3 and τ_3. To simplify the EW propagation model, we use the following notations, $\{air \rightarrow wheat\} : \{\Psi_1, \tau_1\}$, $\{wheat \rightarrow air\} : \{\Psi_2, \tau_2\}$, and $\{wheat \rightarrow copper\ plate\} : \{\Psi_3, \tau_3\}$.

The three-layer model provides the basis for the RF sensing design in this study. Next, we discuss the theoretical foundation of TagSense.

D. Distance-Independent Impedance Algorithm

From the previous discussion, it can be seen that although load impedance can be obtained using the reflection coefficient at position O, it is an weak feature as it is affected by distance d. However, if we can obtain the reflection coefficient for the tag position, we could indirectly obtain the tag's impedance. Thus, the tag's impedance will not be related to distance d anymore (since $d = 0$ now), but only to the surroundings of the tag. Motivated by this observation, we propose a Fresnel reflection coefficient algorithm in this section.

1) Fresnel Reflection Coefficient: According to the electromagnetic reflection theory [36], we have

$$\Psi_1 = \frac{Z_{chip} - Z_d^*}{Z_{chip} + Z_d}, \tag{7}$$

where Ψ_1 denotes the reflection coefficient at the boundary of layer 1 and layer 2, i.e., Fresnel reflection coefficient of the tag from *wheat* $\rightarrow$ *air*; Z_{chip} is the impedance of the chip, which takes a constant complex value; and Z_d is the tag's impedance.

The S_{11} parameter of Port 1 can be expressed as

$$S_{11} = \frac{Ef_{1r}}{Ef_{1i}} = \Psi_1 + \frac{\tau_1\tau_2\Psi_3 e^{-2\gamma l}}{1-\Psi_2\Psi_3 e^{-2\gamma l}}, \tag{8}$$

where l denotes the thickness of the container (in meters), γ is the propagation constant, which is usually a complex number. Define $F(l) = e^{-2\gamma l}$ and $\tau = \tau_1\tau_2$. Then (8) can be simplified as

$$S_{11} = \Psi_1 + \frac{\tau\Psi_3 F}{1-\Psi_2\Psi_3 F}, \tag{9}$$

where Ψ_2 and Ψ_3 denotes the reflection coefficient from *wheat* $\rightarrow$ *plate* and the reflection coefficient from *plate* $\rightarrow$ *wheat*, respectively.

We have now established the model for the S-parameter and Ψ by (9), which does not involve distance d. Therefore, if we use Ψ to obtain the impedance value, it will not vary with the distance. Next, we present the distance-independent impedance algorithm based on Ψ.

2) Distance-Independent Algorithm: The Ψ-based distance-independent impedance derivation algorithm consists of the following steps.

Step 1: The reflection coefficient and transmission coefficient at the boundary of {air$\rightarrow$wheat} and {wheat$\rightarrow$air} are $\{\Psi_1, \tau_1\}$ and $\{\Psi_2, \tau_2\}$, respectively. Let η_{ai} and η_{wh} denote the air and wheat dielectric constants. We have

$$\Psi_1 = \frac{\sqrt{\eta_{ai}}-\sqrt{\eta_{wh}}}{\sqrt{\eta_{ai}}+\sqrt{\eta_{wh}}} = \frac{1-\sqrt{\eta_{wh}}}{1+\sqrt{\eta_{wh}}} \tag{10}$$

$$\tau_1 = \frac{2\sqrt{\eta_{ai}}}{\sqrt{\eta_{ai}}+\sqrt{\eta_{wh}}} = \frac{2}{1+\sqrt{\eta_{wh}}}, \tag{11}$$

since $\eta_{ai} = 1.0005898 \pm 0.0000005 \approx 1$ at normal pressure and temperature. Similar to (11), the parameter τ_2 is expressed as

$$\tau_2 = \frac{2\sqrt{\eta_{wh}}}{\sqrt{\eta_{ai}}+\sqrt{\eta_{wh}}} = \frac{2\sqrt{\eta_{wh}}}{1+\sqrt{\eta_{wh}}}. \tag{12}$$

It follows (10), (11), and (12) that

$$\Psi_1^2 = 1-\tau_1\tau_2. \tag{13}$$

Recall that Ψ_1 is the reflection coefficient of {air $\rightarrow$ wheat}, while Ψ_2 is the reflection coefficient of {wheat $\rightarrow$ air}. We thus have $\Psi_1 = -\Psi_2$, where the negative sign indicates the opposite direction.

Step 2: A copper plate is placed behind the wheat container. When the wave incident on the surface of the copper plate, it will be completely reflected due to the high reflectivity of metal. Thus we have $\Psi_3 = -1$. According to (8) and (9), the S-parameter on the copper surface is given by

$$S'_{11} = \frac{Ef_{1r}}{Ef_{1i}} = \Psi_1 - \frac{\tau F}{1-\Psi_1 F}. \tag{14}$$

Step 3: Another scenario is when the copper plate is removed, and the signal penetrates the wheat and enters into the air behind the container, i.e., {wheat $\rightarrow$ air}, and thus we have $\Psi_1 = -\Psi_3$. According to (9), the S-parameter S''_{11} can be written as

$$S''_{11} = \frac{Ef_{1r}}{Ef_{1i}} = \Psi_1 + \frac{\tau\Psi_3 F}{1-\Psi_2\Psi_3 F} = \Psi_1 - \frac{\tau\Psi_1 F}{1-\Psi_1^2 F}. \tag{15}$$

Step 4: Putting (13), (14), and (15) together, we have

$$\begin{cases} S'_{11} = \Psi_1 - \frac{\tau F}{1-\Psi_1 F} \\ S''_{11} = \Psi_1 - \frac{\tau\Psi_1 F}{1-\Psi_1^2 F} \\ \Psi_1^2 = 1-\tau_1\tau_2 = 1-\tau. \end{cases} \tag{16}$$

The S-parameters S'_{11} and S''_{11} are known, since they can be measured by the VNA/reader device. There are three equations with three unknown variables, so the tag Fresnel reflection coefficient Ψ_1 can be solved from (16), and the impedance of the tag can be computed as in (7), which is independent of the distance d.

E. Angle-Agnostic Method

As discussed, the tag angle is another major factor affecting the accuracy of impedance measurement. To make TagSense work steadily at any tag angle, we propose an angle-agnostic method based on multi-class SVM in this section.

1) Circular Polarization Antenna: A polarization of the antenna can be used to infer the direction of the electric field intensity when the antenna radiates, which describes the parameters of the spatial direction of the wave vector radiated. Specifically, the circular polarization antenna is used in this study, which can receive the level value at any direction of linear polarization. A suitable beam width can reduce the sensitivity of the tag to the angle in space. The angle-agnostic method leverages a circular polarization antenna with a beamwidth of 65° to achieve sufficient resilience to different tag angles, thus reducing the dependence of the system on tag angle.

2) Multi-Class SVM: In addition to using the polarized antenna, we propose a multi-class SVM model to further mitigate the dependency on tag angle. We construct M binary SVMs, termed one-against-the-rest (each one class is corresponding to a certain moisture level). Each binary SVM is constructed to separate a class n from the other $(M-1)$ classes, by solving the following quadratic programming problems.

$$\min_{w_t^n, w_h^n, \xi^n} \quad \frac{1}{2}\left(w_t^n\right)^T w_t^n + C\sum_{t=1}^{N}\xi_t^n \tag{17}$$

$$\text{s.t.} \quad \left(w_t^n\right)^T O(X_t) + w_h^n \geq 1-\xi_t^n \tag{18}$$

$$\left(w_t^n\right)^T O(X_t) + w_h^n \geq -1+\xi_t^n \tag{19}$$

$$\xi_t^n \geq 0, \tag{20}$$

where subscript t is the index of samples and superscript $n \in \{1, 2, 3, \ldots, M\}$ is the index of classes; w_t and w_h are the weight parameters of the hyperplane; ξ is Lagrange multiplier; C is a constant; and $O(X_t)$ represents the optimal hyperplane function of sample X_t.

The M binary SVMs are trained by solving the quadratic programming problems with n variables. In this study, we set

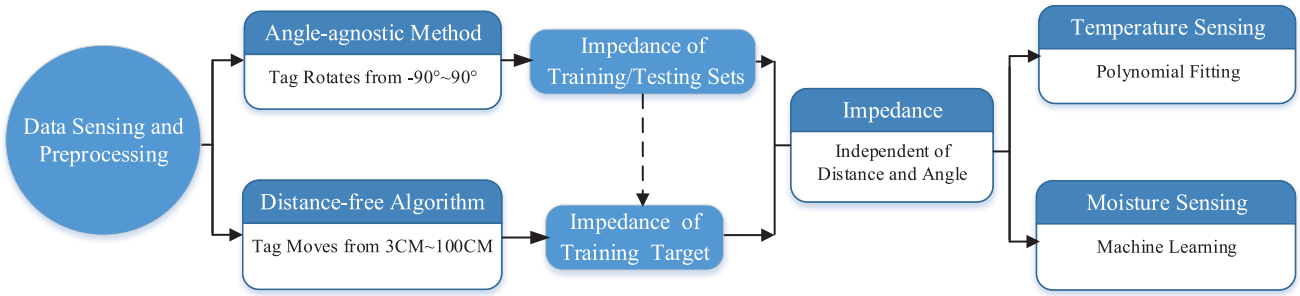

Fig. 10. Algorithm flow chart of TagSense, with the proposed distance-independent and angle-agnostic methods to obtain a stable impedance value, which is then used to determine the temperature and moisture level of the wheat sample.

$M = 10$ (different moisture levels) for wheat samples with different tag rotation angles (from $-\pi/2$ to $\pi/2$). The decision function is given by

$$f(X_{new}) = \underset{n\in\{1,\ldots M\}}{\operatorname{argmax}} \left\{ \sum_{X_t \in\ s_v} y_t \alpha_t^n \kappa \langle X_t, X_{new} \rangle + w_h^n \right\}, \quad (21)$$

where s_v stands for the support vectors, $\kappa\langle\cdot,\cdot\rangle$ is the kernel function, α is a dimensional weight vector, and y is an augmented vector of samples. If a new data sample X_{new} achieves the largest value for class n ($n = 1, 2, 3, 4, 5, \ldots 10$), then $f(x) = n$ and X_{new} will be classified to class n. The multi-class classification includes the following six steps.

Step 1: TagSense collects data from different angles and at different distances, to establish a sample database for training.

Step 2: The tag's impedance measured at 0° is set as the training target.

Step 3: The input data is normalized to the range of [0, 1].

Step 4: The Gaussian radial basis function (RBF) is used as kernel function, and the model parameters are initialized.

Step 5: The SVM is trained using a randomly selected dataset, while 60% of data is used for training, 20% of data with noise is used for retraining to make the model more robust, and 20% of data is used for testing.

Step 6: The trained model is used for classification of a new tag's impedance sample at a random angle.

F. Temperature and Moisture Sensing

Through the distance-independent algorithm, we obtain a stable tag impedance value disregarding the distance d. Through the angle-agnostic method, we reduce the impact of tag angle. Then, the stable impedance value will be obtained, which is used to determine the temperature and moisture level of the wheat sample.

For temperature sensing, we measured the tag impedance at different temperatures and obtained a mathematical model for predicting temperature through polynomial fitting. For wheat moisture sensing, because there is no clear linear relationship between tag impedances and sample moisture levels, we consider using a machine learning method to predict the moisture content. Due to the simple structure of the multi-class SVM, overfitting is less likely when dealing with small datasets. Therefore, the multi-class SVM is also used to predict wheat moisture. TagSense collects tag impedances of wheat at different moisture content levels. To enrich the dataset, TagSense collects tag impedances of the same moisture levels from various angles. It then utilizes the collected tag impedance as training data and wheat moisture levels as the training target to train a model for predicting unknown wheat moisture. The algorithm flow chart is given in Fig. 10, it presents the process of the algorithm design.

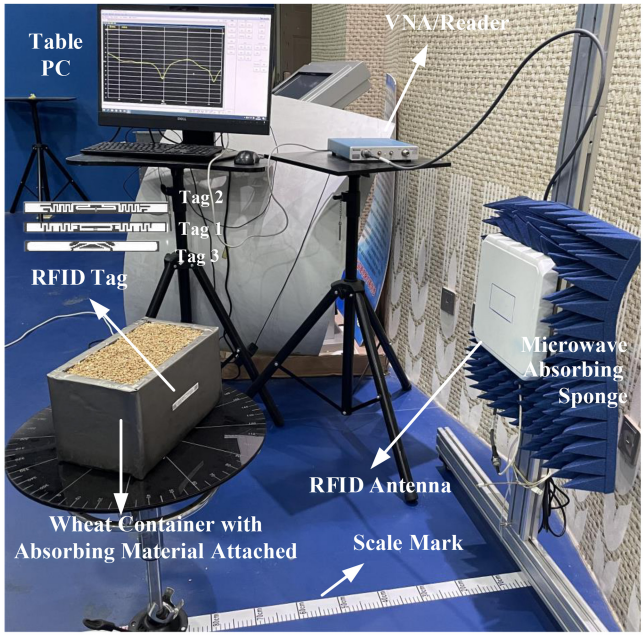

Fig. 11. TagSense experiment configuration.

IV. Experiments and Results

A. TagSense Deployment

The TagSense system consists of a passive RFID tag (Higgs 3 chip of Alien NO.9640), a receiving/transmitting antenna (S9028 PCR of Laird_2), an analog VNA/RFID reader device (Model TTR506A of Tektronix), a desktop computer, and a 1 mm thick copper plate (which is removable). The copper plate is used as a reflective device, which can be easily removed during the experiments. A container made of organic glass is used to hold wheat samples, with a size of 31.5 × 18.0 × 18.0 cm^3. The tag is attached to the outside of the container facing the reader antenna. As shown in Fig. 11,

in order to eliminate or reduce interference, the container is covered with RF absorbing material, leaving an opening of the same size as the tag at the place where the tag is attached. The absorbing material can effectively absorb signals with frequencies ranging from 100 MHz to 6 GHz. This configuration helps to minimize the impacts of both container size and wheat sample cross-sections on the system performance.

The container is placed in the sensing area on a rotating table. The distance between the antenna and the tag is varied from 3 cm to 100 cm. The tag communicates with the reader antenna, and the reader antenna is connected to the VNA/reader device through a cable. The VNA/reader device measures the S-parameter and frequency from received tag response signals, and then sends the measured data to the computer for preprocessing and visualization. The antenna communicates with the tag on different frequency channels (ranging from 860 MHz to 960 MHz). As for temperature sensing, the real part of the tag impedance is leveraged to estimate temperature. For moisture sensing, a machine learning method is utilized to identify the moisture level.

B. Robustness Improvement

We conduct extensive experiments in a laboratory at the room temperature about 20°. Wheat samples at different moisture levels are put into the container to which the tag is attached, and the container is rotated from $-\pi/2$ to $\pi/2$ in steps of 5°, while tag impedance is calculated and recorded.

The ten curves in Fig. 12(a) correspond to ten wheat moisture content levels, demonstrating the variations of tag's impedance during the rotation from $-45°$ to $+45°$. Note that there are no intersection of the ten curves in the range from $-27°$ to $+12°$, which means that the system can identify angles well in this range. As the angle increases, there are more intersections, and the system performance will be affected. Therefore, we consider that the system performs the best within $[-27°, +12°]$.

To verify the performance of the distance-independent algorithm, we conduct experiment with distances within 100 cm, and then calculate the tag's impedance at steps of 2 cm. The results of the experiments are plotted in Fig. 12(b), which shows the impedance variations under different distances. It can be seen that the impedance remains around 60 Ω for distances up to 80 cm, while the impedance fluctuates when the distance is larger than 80 cm. Therefore, the TagSense system performs well within a range of 80 cm.

To further validate the system's performance, we selected another two different types of tags, as depicted in Fig. 11 (represented by tags 1 and tag 3). Utilizing the algorithm proposed in this paper, we can obtain stable tag impedance values, as shown in Fig. 12(b). This indicates that once the tag is activated by the system and establishes communication with the RFID reader, the system can obtain tag impedance values, which can then be utilized to map the target's information.

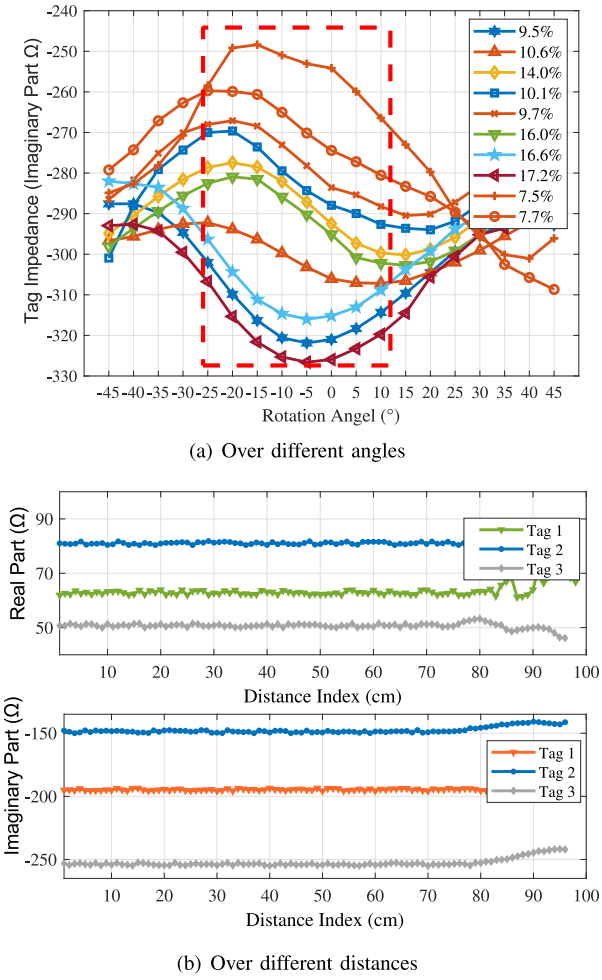

(a) Over different angles

(b) Over different distances

Fig. 12. Tag's impedance over various distances and angles.

C. Moisture and Temperature Sensing Results

Once a stable impedance measurement is obtained, we can use it as a feature to infer the properties of wheat, such as temperature and moisture. Wheat samples at moisture levels of {7.5%, 7.7%, 9.5%, 9.7%, 10.1%, 10.6%, 14.0%, 16.0%, 16.6%, 17.2%} are used to conduct this experiment. The room temperature is set to 20°. We randomly put ten kinds of wheat samples with different moisture contents in the sensing area, and obtain ten impedance measurements (taking the real part as an example). Fig. 13(a) presents the tag's impedances versus moisture levels. We find that the variation of tag impedance is consistent with the moisture level, i.e., the impedance increases with the increase of moisture level. Therefore, we use tag's impedance to characterize wheat moisture.

We next examine the other properties of wheat, i.e., temperature. The wheat moisture level of 14.0% is taken as an example here. We put the wheat sample into a refrigerator to freeze it to -10°C. The laboratory room temperature is set to 20°C. Then the wheat sample is taken out of the refrigerator and placed in the sensing area. We record the tag's impedance until its temperature rises to 20°C. Fig. 13(b) represents the relationship between temperature and the real

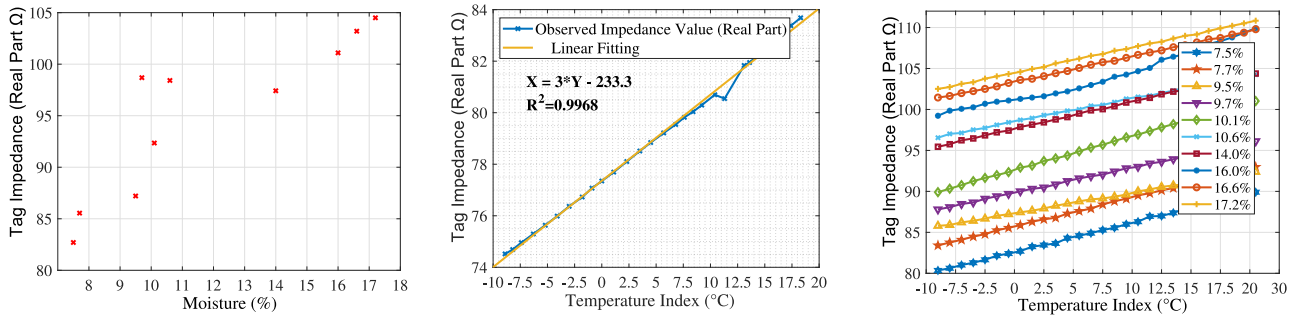

(a) The relationship between the moisture level of ten wheat samples and tag's impedance: the impedance increase with the moisture level.

(b) The linear relationship between temperature and tag's impedance (the real part), taking wheat with the 14.0% moisture level as an example.

(c) With the increase of temperature, the tag's impedance of ten moisture levels all increases roughly linearly.

Fig. 13. Wheat moisture and temperature versus tag impedance at the resonance frequency.

TABLE I
ACCURACY OF DETECTING TEN MOISTURE LEVELS AT VARIOUS SENSING ANGLES

	Moisture Content Level										
Angle Range	7.5%	7.7%	9.5%	9.7%	10.1%	10.6%	14.0%	16.0%	16.6%	17.2%	Average
0°	100.0%	100.0%	100.0%	100.0%	100.0%	100.0%	100.0%	100.0%	100.0%	100.0%	100.0%
$-\pi/6$ to $+\pi/6$	96.2%	95.9%	97.5%	98.5%	100.0%	100.0%	100.0%	100.0%	100.0%	94.8%	98.6%
$-\pi/4$ to $+\pi/4$	95.5%	94.6%	100.0%	98.7%	98.1%	99.5%	92.9%	100.0%	97.6%	94.5%	97.2%
$-\pi/3$ to $+\pi/3$	94.5%	91.2%	97.4%	97.1%	95.2%	99.5%	87.4%	100.0%	93.3%	87.0%	94.4%
$-\pi/2$ to $+\pi/2$	87.5%	86.1%	91.2%	86.7%	92.2%	91.2%	88.1%	100.0%	88.6%	83.6%	89.5%

TABLE II
ACCURACY OF TEMPERATURE SENSING FOR WHEAT SAMPLES WITH DIFFERENT FITTING CURVES

Moisture Level	7.5%	7.7%	9.5%	9.7%	10.1%	10.6%	14.0%	16.0%	16.6%	17.2%
Fitting Curve	Linear	Conic	Linear	Linear	Linear	Linear	Conic	Conic	Conic	Conic
R^2	0.977%	0.994	0.963	0.975%	0.991%	0.9951	0.999	0.999	0.989%	0.997
Error rate	8.7%	3.9%	10.0%	9.2%	6.7%	1.7%	4.4%	4.5%	2.3%	5.12%

part of tag's impedance. It can be seen that there is a strong linear relationship between temperature and tag's impedance. The curve fitting yields $x = 3y - 233.3$, with $R^2 = 0.996$, and the relative error RE is only 4.4%. Note that R^2 is a parameter that represents the performance of data fitting ($R^2 = 1$ indicates a prefect fit).

Table I represents the accuracy of TagSense for ten moisture content levels at various tag angles, as achieved by the angle-agnostic method. We can see that TagSense can achieve a satisfactory accuracy in this experiment. The accuracy is 100% for the moisture content level of 16.0%. When the angle is set from $-\pi/2$ to $+\pi/2$, TagSense still achieves the minimum accuracy of 83.6%, which is a satisfactory result. Table II presents the accuracy of temperature sensing for wheat using different fitting curves, where a Conic curve is given by $ax^2 + bxy + cy^2 + dx + ey + f = 0$, and a Linear curve is given by $y = ax + b$. From the above two tables and Fig. 13(c), we conclude that tag's impedance can well represent the trend of temperature, with a fitting accuracy higher than 0.96.

Fig. 14 presents a 3D graph of wheat moisture, temperature, and tag's impedance. We project red triangular marks and yellow circular marks on the X_Z plane (i.e., temperature vs tag impedance) and the Y_Z plane (i.e., moisture vs tag impedance), respectively. It shows that the impedance increases with temperature at the resonance frequency, and

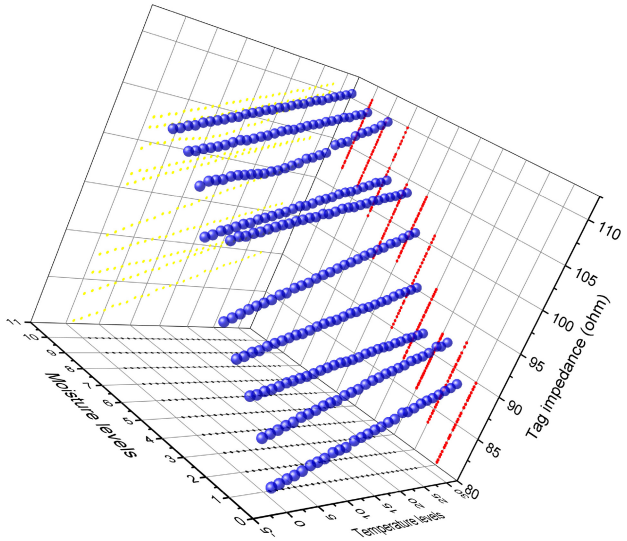

Fig. 14. The relationship among temperature, moisture, and tag impedance at frequency of 942.5 MHz.

indicates there is a linear relation for temperature and impedance on the X_Z plane. Also, the slopes of corresponding curves over different moisture contents are similar. For the Y_Z plane, as the increase of moisture, tag impedance

TABLE III
COMPARISONS OF DIFFERENT RFID-BASED SENSING SYSTEMS

Technique	Temperature Error	Other Application	Features	Costs	Robust to environment	Online	Off-the-shelf
RFIDHacking [26]	10°C	Gesture	Differential Minimum Response Threshold	medium	Not mentioned	Yes	No
RFThermometer [28]	5°C	NO	Phase	medium	Not mentioned	Yes	Yes
RTSense [29]	2.9°C	NO	Tag Impedance Phase Difference	Low	Yes	Not mentioned	Yes
Thermotag [37]	2.7°C	NO	Discharging Period of Tag' Chip	Low	Yes	Not mentioned	No
TagSense (proposed)	1.1°C	*Moisture*	*Tag Impedance with Resonance Frequency*	*Low*	*Yes*	*Yes*	*Yes*

approximately increases, but the linear relationship is not obvious.

In order to demonstrate the efficacy of the TagSense system, Table III presents our comparison study with other four baseline systems. It can be seen that all the five systems can sense wheat temperature, but TagSense achieves the highest accuracy with an average error of 1.1°C. Furthermore, only RFIDHacking [26] and TagSense can sense temperature as well as other properties of the target, such as gesture and moisture. Specifically, TagSense uses tag's impedance to sense the target property, which helps to obtain more stable features, making it robust to environmental interference. The RFID based systems also have the advantages of having a low cost and robust to environmental dynamics and interference. All the four systems can be used for online testing. The RFThermometer [28], RTSense [29], and the proposed TagSense systems have the desirable advantage of using off-the-shelf devices.

V. CONCLUSION

In this work, we presented the TagSense system for contact-less sensing target's properties (i.e., moisture level and temperature) using a single passive RFID tag. We validated the feasibility of using tag's impedance as a feature to sense the target, and then developed the TagSense framework, including data acquisition, data pre-processing, SVM-based classification, and temperature and moisture determination. To mitigate the influence of distance and angle, a distance-independent algorithm and an angle-agnostic method were proposed for robust sensing performance. Our extensive experiments validated that the system can obtain a stable impedance at any angle and distance within the sensing area, which can be used as a feature to accurately infer target properties such as moisture level and temperature.

REFERENCES

[1] R. Chandra, "FarmBeats: An IoT system for agriculture," in *Proc. USENIX NSDI*, 2016, pp. 515–529.
[2] S. Sokhansanj and W. Yang, "Technical notes: Revision of the ASAE standard D245.4: Moisture relationships of grains," *Trans. Am. Soc. Agric. Biol. Eng.*, vol. 39, no. 2, pp. 639–642, Feb. 1996.
[3] W. C. Wang and Y. Z. Dai, "A grain moisture detecting system based on capacitive sensor," *Int. J. Digit. Content Technol. Appl.*, vol. 5, no. 3, pp. 203–209, Mar. 2011.
[4] Z. Xiang, J. Wu, C. Qi, and X. Hu, "Contactless detection of moisture content in blended fabrics with a free-space microwave method," *IEEE Trans. Instrum. Meas.*, vol. 69, no. 5, pp. 2139–2144, May 2020.
[5] F. Gan, Z. Liu, W. Zhang, L. Ming, R. Wang, and F. Jiang, "Development of grain moisture detecting instrument based on friction resistance method," *J. Agric. Mech. Res.*, vol. 20, no. 15, p. 4102, Aug. 2018.
[6] Y. Y. Q. Yang YueQian, W. J. P. Wang JianPing, and W. C. Z. Wang, "Study on on-line measurement of grain moisture content by neutron gauge," *Trans. Chin. Soc. Agric. Eng.*, vol. 16, no. 5, pp. 99–101, 2000.
[7] P. Hu, W. Yang, X. Wang, and S. Mao, "MiFi: Device-free wheat mildew detection using off-the-shelf WiFi devices," in *Proc. IEEE GLOBECOM*, 2019, pp. 1–6.
[8] W. Yang, X. Wang, A. Song, and S. Mao, "Wi-wheat++: Contact-free wheat moisture detection using commodity WiFi," in *Proc. IEEE ICC*, 2018, pp. 1–6.
[9] P. Hu, W. Yang, X. Wang, and S. Mao, "Contract-free wheat mildew detection using commodity WiFi," *Elsevier/KeAi Int. J. Cogn. Comput. Eng.*, vol. 3, no. 1, pp. 9–23, Jan. 2022.
[10] A. Bekkali, S. Zou, A. Kadri, M. Crisp, and R. V. Penty, "Performance analysis of passive UHF RFID systems under cascaded fading channels and interference effects," *IEEE Trans. Wireless Commun.*, vol. 14, no. 3, pp. 1421–1433, Mar. 2015.
[11] A. Abuelkhail, U. Baroudi, M. Raad, and T. Sheltami, "Internet of Things for healthcare monitoring applications based on RFID clustering scheme," *Wireless Netw.*, vol. 27, pp. 747–763, Nov. 2021.
[12] B. Xie et al., "Tagtag: Material sensing with commodity RFID," in *Proc. ACM SenSys*, 2019, pp. 338–350.
[13] P. Yang, Y. Feng, J. Xiong, Z. Chen, and X.-Y. Li, "RF-Ear: Contactless multi-device vibration sensing and identification using COTS RFID," in *Proc. IEEE INFOCOM*, 2020, pp. 297–306.
[14] P. K. Singh, N. Kumar, and B. K. Gupta, "Wireless sensing with radio frequency identification (RFID): Instrumental in intelligent tracking," in *Proc. ICRIC*, 2021, pp. 345–356.
[15] D. Zhong and F. Liu, "RF-OSFBLS: An RFID reader-fault-adaptive localization system based on online sequential fuzzy broad learning system," *Neurocomputing*, vol. 390, pp. 28–39, May 2020.
[16] D. Li, B. Zhang, and C. Li, "A feature-scaling-based k-nearest neighbor algorithm for indoor positioning systems," *IEEE Internet Things J.*, vol. 3, no. 4, pp. 590–597, Aug. 2015.
[17] G. Wang et al., "HMO: Ordering RFID tags with static devices in mobile environments," *IEEE Trans. Mobile Comput.*, vol. 19, no. 1, pp. 74–89, Jan. 2020.
[18] Y. Bu et al., "RF-dial: Rigid motion tracking and touch gesture detection for interaction via RFID tags," *IEEE Trans. Mobile Comput.*, vol. 21, no. 3, pp. 1061–1080, Mar. 2022.
[19] L. Pu, H.-C. Wu, K. Yan, Z. Gao, X. Wang, and W. Xiang, "Novel three-hierarchy multiple-tag-recognition technique for next generation RFID systems," *IEEE Trans. Wireless Commun.*, vol. 19, no. 2, pp. 1237–1249, Feb. 2020.
[20] U. Ha, J. Leng, A. Khaddaj, and F. Adib, "Food and liquid sensing in practical environments using RFIDs," in *Proc. USENIX NSDI*, 2020, pp. 1083–1100.
[21] R. Melo, J. Silva, and I. S. Queiroz, "Radio frequency identification in Internet of underground things using a soil dielectric attenuator and microstrip antenna as tag sensor," *Wiley Microw. Opt. Technol. Lett.*, vol. 63, no. 9, pp. 2408–2413, Sep. 2021.

[22] S. Christoph, J. Sergej, M. Maximilian, and B. Matthias, "Moisture measurements with RFID based sensors in screed and concrete," in *Proc. 8th Eur. Workshop Struct. Health Monit.*, 2016, pp. 1–10.
[23] T. Theophanous, "Moisture measurements in concrete and characterization using impedance spectroscopy and RC network circuits," Ph.D. dissertation, Dept. Eng. Sci. Mech., Virginia Polytech. Inst., Blacksburg, VA, USA, Aug. 2008.
[24] N. Azmi, L. M. Kamarudin, A. Zakaria, D. L. Ndzi, and L. Mohamed, "RF-based moisture content determination in rice using machine learning techniques," *MDPI Sens.*, vol. 21, no. 5, p. 1875, Mar. 2021.
[25] Z. Zhu, Y. Huang, Z. Chen, and H. Huang, "Non-contact infrared temperature detection and RFID technology access control design," *J. Phys., Conf. Ser.*, vol. 1982, no. 1, May 2021, Art. no. 012087.
[26] J. Wang, O. Abari, and S. Keshav, "Challenge: RFID hacking for fun and profit," in *Proc. ACM MobiCom*, 2018, pp. 461–470.
[27] W. Zhu, Q. Zhang, M. Matlin, Y. Chen, and H. Xiao, "Passive digital sensing method and its implementation on passive RFID temperature sensors," *IEEE Sensors J.*, vol. 21, no. 4, pp. 4793–4800, Feb. 2020.
[28] X. Wang, J. Zhang, Z. Yu, S. Mao, S. Periaswamy, and J. Patton, "On remote temperature sensing using commercial UHF RFID tags," *IEEE Internet Things J.*, vol. 6, no. 6, pp. 10715–10727, Dec. 2019.
[29] S. Pradhan and L. Qiu, "RTSense: Passive RFID based temperature sensing," in *Proc. 18th ACM SenSys*, 2020, pp. 42–55.
[30] X. Zhang, H.-X. Li, and S. H. Chung, "Setup-independent sensing architecture with multiple UHF RFID sensor tags," *IEEE Internet Things J.*, vol. 9, no. 2, pp. 1243–1251, Jan. 2021.
[31] E. Shen, W. Yang, X. Wang, S. Mao, and W. Bin, "TagSense: Robust wheat moisture and temperature sensing using a passive RFID tag," in *Proc. IEEE ICC*, 2022, pp. 1–6.
[32] M. Sabina, O. Cecilia, N. Shankar, C. Alexandro, N. Corrado Di, and M. Gaetano, "Humidity sensing by polymer-loaded UHF RFID antennas," *IEEE Sensors J.*, vol. 12, no. 9, pp. 2851–2858, Sep. 2012.
[33] X. Qing, C. K. Goh, and N. C. Zhi, "Impedance characterization of RFID tag antennas and application in tag co-design," *IEEE Trans. Microw. Theory Techn.*, vol. 57, no. 5, pp. 1268–1274, May 2009.
[34] P. M. Rodrigo, E. F. Fernández, M. Theristis, and F. A. Cruz, "Characterization of the spectral matching ratio and the Z-parameter from atmospheric variables for CPV spectral evaluation," *IEEE J. Photovolt.*, vol. 7, no. 6, pp. 1802–1809, Nov. 2017.
[35] D. A. Frickey, "Conversions between S, Z, Y, H, ABCD, and T parameters which are valid for complex source and load impedances," *IEEE Trans. Microw. Theory Techn.*, vol. 42, no. 2, pp. 205–211, Feb. 1994.
[36] D. M. Pozar, *Microwave Engineering*. Hoboken, NJ, USA: Wiley, 2004.
[37] X. Chen, J. Liu, F. Xiao, S. Chen, and L. Chen, "Thermotag: Item-level temperature sensing with a passive RFID tag," in *Proc. ACM MobiSys*, 2021, pp. 163–174.

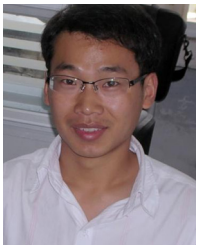

Erbo Shen received the B.S. and M.S. degrees from the School of Information Science and Engineering, Henan University of Technology, China, in 2006 and 2009, respectively, where he is currently pursuing the Ph.D. degree with the School of Mechanical and Electrical Engineering. He is with the Henan Key Laboratory of Grain Photoelectric Detection and Control, Henan University of Technology, Zhengzhou, China, and also with the College of International Education, Kaifeng University, Kaifeng, China. He is currently interested in wireless sensing and smart agriculture.

Weidong Yang (Member, IEEE) received the B.S. degree in industrial automation and the M.S. and Ph.D. degrees in computer science from Xidian University, China, in 1999, 2005, and 2008, respectively. He is currently a Professor with the Henan University of Technology, where he is also the Deputy Chair of the Key Laboratory of Grain Information Processing and Control, Ministry of Education. His research focuses on wireless networks security, privacy protection, and vehicular ad hoc networks. He is a Senior Member of the *China Computer Federation*.

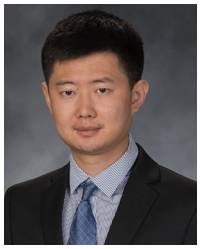

Xuyu Wang (Member, IEEE) received the M.S. degree in signal and information processing, the B.S. degree in electronic information engineering from Xidian University, Xi'an, China, in 2012 and 2009, respectively, and the Ph.D. degree in electrical and computer engineering from Auburn University, Auburn, AL, USA, in August 2018. He is currently an Assistant Professor with the Knight Foundation School of Computing and Information Sciences, Florida International University, Miami, FL, USA. His research interests include wireless sensing, Internet of Things, wireless localization, smart health, wireless networks, and deep learning. He received the NSF CRII Award in 2021. He was a co-recipient of the 2022 Best Journal Paper Award of IEEE ComSoc eHealth Technical Committee, the IEEE INFOCOM 2022 Best Demo Award, the IEEE ICC 2022 Best Paper Award, the IEEE Vehicular Technology Society 2020 Jack Neubauer Memorial Award, the IEEE GLOBECOM 2019 Best Paper Award, the IEEE ComSoc MMTC Best Journal Paper Award in 2018, the IEEE PIMRC 2017 Best Student Paper Award, the IEEE SECON 2017 Best Demo Award, and the Second Prize of the Natural Scientific Award of the Ministry of Education, China, in 2013.

Bo Kang, photograph and biography not available at the time of publication.

Shiwen Mao (Fellow, IEEE) is a Professor, the Earle C. Williams Eminent Scholar, and the Director of the Wireless Engineering Research and Education Center, Auburn University. His research interest includes wireless networks, multimedia communications, and smart grid. He is the Editor-in-Chief of IEEE TRANSACTIONS ON COGNITIVE COMMUNICATIONS AND NETWORKING. He was the General Chair of IEEE INFOCOM 2022, the TPC Chair of IEEE INFOCOM 2018, and the TPC Vice-Chair of IEEE GLOBECOM 2022. He received the IEEE ComSoc MMTC Outstanding Researcher Award in 2023, the SEC (Southeastern Conference) 2023 Faculty Achievement Award for Auburn, the IEEE ComSoc TC-CSR Distinguished Technical Achievement Award in 2019, the Auburn University Creative Research & Scholarship Award in 2018, and the NSF CAREER Award in 2010, and several service awards from IEEE ComSoc. He is a co-recipient of the 2022 Best Journal Paper Award of IEEE ComSoc eHealth Technical Committee, the 2021 Best Paper Award of Elsevier/KeAi Digital Communications and Networks Journal, the 2021 IEEE Internet of Things Journal Best Paper Award, the 2021 IEEE Communications Society Outstanding Paper Award, the IEEE Vehicular Technology Society 2020 Jack Neubauer Memorial Award, the 2018 Best Journal Paper Award, the 2017 Best Conference Paper Award from IEEE ComSoc MMTC, and the 2004 IEEE Communications Society Leonard G. Abraham Prize in the Field of Communications Systems. He is a co-recipient of the Best Paper Awards from IEEE GLOBECOM 2023 (two), 2019, 2016, and 2015, IEEE ICC 2022 and 2013, IEEE WCNC 2015, the Best Demo Awards from IEEE INFOCOM 2022, and IEEE SECON 2017.